Pharmacological Research 194 (2023) 106862

Contents lists available at ScienceDirect

Pharmacological Research

journal homepage: www.elsevier.com/locate/yphrs

An innovative strategy to investigate microbial protein modifications in a reliable fast and sensitive way: A therapy oriented proof of concept based on UV-C irradiation of SARS-CoV-2 spike protein

Sergio Strizzi [a,1], Letizia Bernardo [b,1], Pasqualina D'Ursi [b], Chiara Urbinati [c], Andrea Bianco [d], Fiona Limanaqi [a,e], Andrea Manconi [b], Maria Milanesi [b,c], Alberto Macchi [d], Dario Di Silvestre [b], Adalberto Cavalleri [f], Giovanni Pareschi [d], Marco Rusnati [c], Mario Clerici [e,g], PierLuigi Mauri [b,h,*], Mara Biasin [a]

[a] Department of Biomedical and Clinical Sciences, University of Milan, Via G.B. Grassi, 20122 Milan, Italy
[b] Institute for Biomedical Technologies, National Research Council (ITB-CNR), 20054 Segrate, MI, Italy
[c] Unit of Macromolecular Interaction Analysis, Department of Molecular and Translational Medicine, University of Brescia, 25123 Brescia, Italy
[d] Italian National Institute for Astrophysics (INAF) - Brera Astronomical Observatory, Via E. Bianchi, 46, Merate, 23807 Lecco, Italy
[e] Department of Pathophysiology and Transplantation, University of Milan, Via Francesco Sforza, 20122 Milan, Italy
[f] Epidemiology and Prevention Unit, IRCCS Foundation, Istituto Nazionale dei Tumori, Via Giacomo Venezian, 1, 20133 Milan, Italy
[g] Don C. Gnocchi Foundation, Istituto di Ricovero e Cura a Carattere Scientifico (IRCCS) Foundation, Via A. Capecelatro 66, 20148 Milan, Italy
[h] Interdisciplinary Research Center "Health Science", Sant'Anna School of Advanced Studies, 56127 Pisa, Italy

ARTICLE INFO

Keywords:
UV light
Spike protein
Proteomics
Structural biology

ABSTRACT

The characterization of modifications of microbial proteins is of primary importance to dissect pathogen lifecycle mechanisms and could be useful in identifying therapeutic targets. Attempts to solve this issue yielded only partial and non-exhaustive results. We developed a multidisciplinary approach by coupling *in vitro* infection assay, mass spectrometry (MS), protein 3D modelling, and surface plasma resonance (SPR). As a proof of concept, the effect of low UV-C (273 nm) irradiation on SARS-CoV-2 spike (S) protein was investigated. Following UV-C exposure, MS analysis identified, among other modifications, the disruption of a disulphide bond within the conserved S2 subunit of S protein. Computational analyses revealed that this bond breakage associates with an allosteric effect resulting in the generation of a closed conformation with a reduced ability to bind the ACE2 receptor. The UV-C-induced reduced affinity of S protein for ACE2 was further confirmed by SPR analyses and *in vitro* infection assays. This comprehensive approach pinpoints the S2 domain of S protein as a potential therapeutic target to prevent SARS-CoV-2 infection. Notably, this workflow could be used to screen a wide variety of microbial protein domains, resulting in a precise molecular fingerprint and providing new insights to adequately address future epidemics.

1. Introduction

Effective microbe inactivation mostly depends on pathogen structure and composition [1,2]. Thus, delving into the biological functions of pathogen domains involved in microbial-host cell interaction, assembly and budding is of foremost importance for a better understanding of infectious disease mechanisms. Notably, clarification of the nature of such interactions could also lead to the design of novel pharmacological approaches [3]. This has been addressed using a number of different methodologies, from mass spectrometry (MS) to computational analyses [4,5]. However, none of these methods was able to provide fully satisfactory results.

The recent COVID-19 pandemic driven by SARS-CoV-2 has further emphasised this caveat, and has shown that the world is unprepared to rapidly identify microbial Achilles' heels, delaying the development of effective treatment strategies against the effects of deadly, and

* Corresponding author at: Institute for Biomedical Technologies, National Research Council (ITB-CNR), 20054 Segrate, MI, Italy.
E-mail address: pierluigi.mauri@itb.cnr.it (P. Mauri).
[1] These authors contributed equally to this work.

https://doi.org/10.1016/j.phrs.2023.106862
Received 27 April 2023; Received in revised form 4 July 2023; Accepted 18 July 2023
Available online 20 July 2023
1043-6618/© 2023 Published by Elsevier Ltd. This is an open access article under the CC BY-NC-ND license (http://creativecommons.org/licenses/by-nc-nd/4.0/).

transmissible pathogens. Indeed, actual strategies adopted in the case of a public health emergency are too slow to keep up with pathogen mutation rate, mainly in viral infections [4]. Hence, there is an actual need for a rigorous, and reliable workflow able to promptly define the structural composition and biological functions of microbial domains directly involved in pathogen-host cell interaction, which is a prerequisite for effective, and specific drug design.

The use of computational methods for the analysis of therapeutic viral targets and the discovery of potential drugs has indeed exploded since the beginning of the COVID-19 pandemic. For example, Wu et al. employed Homology modeling and Molecular docking to solve the three-dimensional structures of all the 24 proteins of SARS-CoV-2 and their drug complexes, providing more target information for drug intervention and long-term drug design [4].

The SARS-CoV-2 Spike (S) protein is mainly responsible for virus penetration in human cells following angiotensin-converting enzyme 2 (ACE2) receptor binding [6]. Thus, S protein, in particular its S1-RBD domain, represents the main target for vaccine formulation; however, the use of covalent Spike protein inhibitors has recently emerged as a therapeutically effective strategy as well. This is the case of peptides that interrupt the RBD–ACE2 interaction, interfere with the cleavage of S protein, and block the HR1–HR2 interaction from forming a fusion-active core, or mAbs that target the S protein [7]. Again, these include small molecules, such as amiodarone, which blocks the *in vitro* spread of SARS-CoV by inhibiting virus infection at a post-endosomal level [8], or tetra-O-galloyl-beta-D-glucose (TGG) and luteolin, which block SARS-CoV or SARS pseudovirus entry into Vero E6 cells [9]. More recently, Wang et al. adopted a workflow based on cryo-EM and SILCS Simulation, followed by Structure-Based Hierarchical Virtual Screening and Surface Plasmon Resonance (SPR) to identify small molecule modulators against the FFA-binding pocket of SARS-CoV-2 S protein [3]. Again, MS analysis as well as combined, state-of-the art methodological investigations have been used to investigate the binding sites involved in the specific interaction domains [10,11] and/or to dissect virus-host interaction mechanisms [12,13]. For instance, Lai et al. used complementary approaches to demonstrate the existence of potential antigenic cross-reactivity between S1-RBD and its receptor ACE2 [14].

Notwithstanding, the emergence of new viral mutations and strains progressively limits the effectiveness of pre-existing drugs/vaccines [15,16], claiming for a continuous development of novel ones. This pushed us towards the conception of a pipeline which might be useful to address the present but also future challenges. Indeed, beyond SARS-CoV-2, similar approaches could be applied to all viruses presenting peplomers on their surfaces, such as other coronaviruses (hOC-43, hNL-63, MERS-CoV, SARS-CoV-1), viruses belonging to the family of Paramyxoviridae, or some retroviruses.

Here, we propose an unbiased/multidisciplinary roadmap coupling *in vitro* infection assay, MS, protein 3D modelling and SPR to thoroughly dissect and identify microbe molecular domains that could be potential therapeutic targets (Fig. 1). The methods combined in this pipeline confirm and expand the results obtained by each of them individually, so as to depict a comprehensive prospective of the molecular and functional role of the identified target. As a proof of concept, we investigated the effect of low UV-C irradiation (273 nm) on the SARS-CoV-2 S protein. Indeed, as previously documented by fluorescence *in situ* hybridization (FISH) experiments, UV-C treatment does hamper SARS-CoV-2 ability to infect susceptible cells [17]. This occurs probably by damaging viral proteins (capsid/receptors) that are involved in the recognition of target host cells and absorb in the same spectral range [18,19]. Yet, the molecular domains affected by UV-C radiations, their role in enabling SARS-CoV-2 infection, and the possibility to exploit them in the setting up of new therapeutic strategies have not been investigated so far.

By integrating results obtained through this comprehensive approach, we expect to build a pipeline facilitating the identification and prioritization of candidate targets suitable for novel drug development. Our goal is to provide a reliable, time- and money-saving workflow that could help investigators to quickly answer complex biological questions about protein-protein interactions in the frame of target identification and/or drug discovery.

2. Materials and methods

2.1. Experimental design

As shown in Fig. 1, SARS-CoV-2 infection/replication capability was assessed in an *in vitro* infection assay following exposure to different UV-C irradiance intensities. Once set up/optimized the protocol of UV-C ray administration, dosage, and timing (Fig. lA), the molecular modifications induced by UV-C exposure on the Spike (S) protein were investigated by different approaches: i) characterization by MS; ii) S modelling and structural dynamics; and iii) affinity receptor binding by SPR analysis (Fig. 1B).

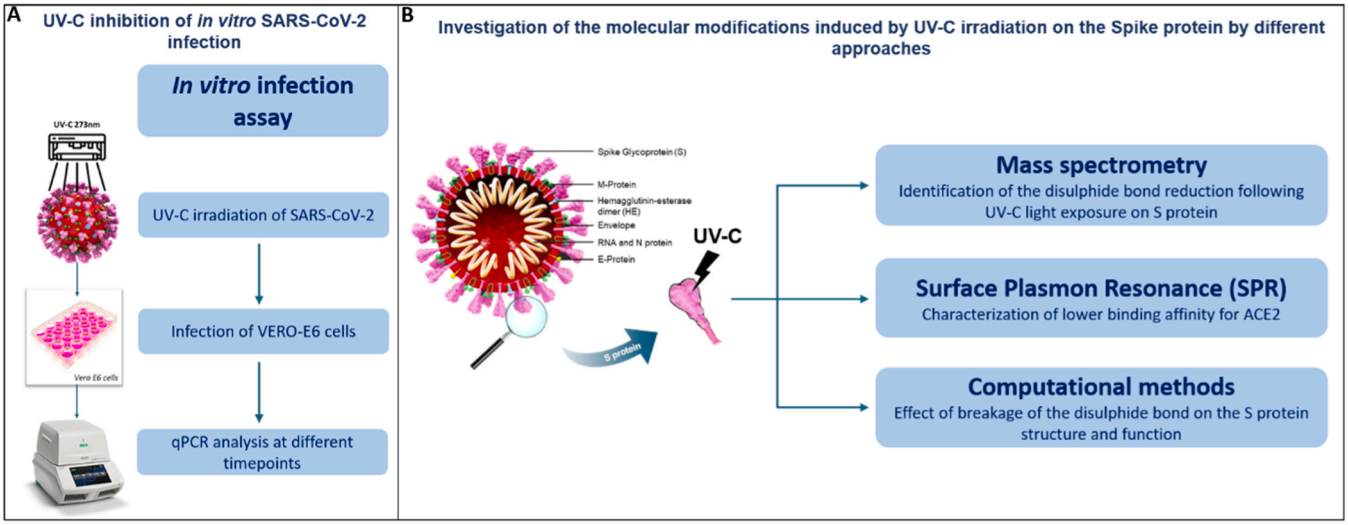

Fig. 1. General flow chart of the experimental work. Graphical representation of the multidisciplinary approach adopted to assess how UV-C irradiation affects SARS-CoV-2 S protein. (A) SARS-CoV-2 *in vitro* infection assay to set-up UV-C ray administration, dosage, and timing; (B) analyses of UV-C induced effect on the S protein, by mass spectrometry (MS), surface plasma resonance (SPR) and computational methods involving modelling and structural dynamics.

2.2. Cell lines, virus, and reagents

VeroE6 cells (CRL-1586™, African green monkey kidney epithelial cells), purchased from American Type Culture Collection (ATCC®, Manassas,VA, USA) were grown in DMEM high glucose (ECB20722L, Euroclone, Milan, Italy), supplemented with 10% FBS, and 1% L-Glutamine (LG) and Penicillin Streptomycin (PS). Cells were grown at 37 °C in 5% CO_2 and at 98% humidity. Cells were routinely checked for mycoplasma contamination by PCR test. Cells between passages 15 and 25 were used for the experiments. SARS-CoV-2 Virus Human 2019-nCoV (strain 2019-nCoV/Italy-INMI1, Rome, Italy) was expanded in VeroE6 cells and infectious viral particle concentration was assessed by $TCID_{50}$ endpoint dilution assay as previously described [20]. Recombinant SARS-CoV-2 S protein was purchased from R&D Systems (Cat. N. 10549-CV, R&D Systems biotechne, Minneapolis, MN, USA. Peptide Array, SARS-Related Coronavirus 2 S Glycoprotein was obtained from BEI Resources NIAID, NIH (Cat. N. NR-52402, BEI Resources; www.beiresources.org). Human ACE2 protein was purchased from AcroBiosystems (Newark, DE). Carboxy-methyl dextran CM5 sensorchip, 1-ethyl-3-(3-diaminopropyl)-carbodiimide hydrochloride (EDC) and N-hydroxysuccinimide (NHS) were purchased from Cytiva (Marlborough, MA). Bovine Serum Albumin (BSA) was purchased from Merck (Darmstadt, Germany).

2.3. UV-C treatment at different irradiance/time combinations

To evaluate the relationship between UV-C irradiance intensity and SARS-CoV-2 inhibition, we performed an UV-C illumination test followed by an *in vitro* SARS-CoV-2 infection assay.

VeroE6 cells were seeded in 24-well plates ($2{,}5 \times 10^5$ cells/well), and cultured in complete medium (DMEM with 10% FBS, 1% LG and PS) for 24 h before viral infection assay. SARS-CoV-2 at $1.5 \times 10^3 TCID_{50}$ was irradiated using a custom-made UV lamp equipped with UV-C LEDs peaking at 273 nm and delivering a maximum irradiance of 0.15 mW/cm^2. The total irradiation dose to be delivered before viral inoculum into VeroE6 cells was set at about 4 mJ/cm^2, which was provided through different irradiance-exposure/time combinations (Table 1). The illumination of the virus suspension, as well as the *in vitro* infection assay were performed as previously described [17,21]. UV^- virus served as positive control in each test, considering the large difference in the exposure times. Viral replication in culture supernatants was assessed by an integrated culture-polymerase chain reaction [22] at 1, 2 and 7 dpi, while infected cells were harvested for RNA isolation at 7 dpi. Viral RNA was quantified as previously described [17,21].

2.4. UV-C (273 nm) irradiation of SARS-CoV-2 S protein

A recombinant S protein (S; see Reagents paragraph 2.2 for details) was used to perform UV-C light irradiation. In detail, the same amount of protein (5 μg) was employed for UV^- and UV^+ S experiments, which were performed concurrently. The UV^+ sample was obtained by S illumination with the same lamp used for the virus suspension irradiance tests (UV-C LEDs at 273 nm) with minor modifications. In particular, irradiation experiments were performed setting UV-C lamp at 100% intensity power and the LED-sample distance was minimized to increase the maximum irradiance and reduce the exposure time to 10 s. This precaution was necessary to avoid as much as possible the solvent evaporation during the test. Both UV^- and UV^+ samples were immediately digested with 100 ng of trypsin (Sequencing Grade Modified Trypsin, Porcine, Promega) with a used ratio of 1:50 at 37 °C for three hours. In order to stop digestion, the obtained peptide mixture was diluted in 0.1% formic acid solution (pH <2) and 0.6 μg was injected for each liquid chromatography-MS (nLC-MS) analysis. For proteomic analysis, selected synthetic peptides and a S synthetic library (see Reagents paragraph 2.2. for details) were subjected to UV-C irradiation and immediately analysed by nLC-MS avoiding the digestion step.

Table 1
Different combinations in irradiance fraction and time exposure employed for the *in vitro* SARS-CoV-2 infection assay.

Wavelength (nm)	Irradiance (% of the maximum value)	Exposure time (sec)
273	5	540
273	20	135
273	100	27

2.5. nLC-MS analysis

The tryptic S peptide mixtures were analysed by the Eksigent nanoLC-Ultra® 2D System (Eksigent, AB SCIEX Dublin, CA, USA) configured in trap-elute mode as previously described [23] through a 70 min gradient of eluent B (eluent A, 0.1% formic acid in water; eluent B, 0.1% formic acid in acetonitrile).). Briefly, 600 ng of digested S protein was loaded on a first trap (200–500 μm ChromXP C-18-CL, 3 μm, 120 Å) and then eluted on a reverse-phase nano-column (75 μm x 15 cm ChromXP C18-CL, 3 μm, 120 Å) at a flowrate of 300 nL/minute. The peptide mixtures were separated according to specific gradients (from 5% to 10% B in 2 min, 10–60% B in 38 min, 60–95% B in 8 min and holding in 95% B for 9 min before returning at 5% B in 3 min) and analysed by LTQ-OrbitrapXL mass spectrometer (Thermo Fisher Scientific, Waltham, CA, USA) equipped with a nanospray ion source which were managed by Xcalibur software version 1.4 (Thermo Fisher Scientific, Waltham, CA, USA). Full mass spectra were acquired at 400–1600 *m/z* scan range in positive ion mode and with a resolution setting of 60000 FWHM (@ *m/z* 200) and a scan rate of 2 spectra/-second. The full MS was followed by five low-resolution MS/MS events that were sequentially generated in a data-dependent manner on the top five ions selected from the full MS spectrum (at 35% collision energy), with an isolation window of 2 *m/z* from the survey scan.

Protein quantification was based on the Peptide Spectrum Match (PSM) as widely used for label-free proteomics, specifically for differential analysis, comparing the PSMs of proteins or peptides between two or more conditions [24–27]. The experimental spectra were analysed by Protein Discoverer 2.1 software (Thermo Fisher Scientific, Waltham, CA, USA), with Sequest HT search engine [28] against NCBI sequence YP_009724390 (surface glycoprotein [Severe acute respiratory syndrome coronavirus 2]) retrieved from UNIPROT database (www.uniprot.org) on July 2021 and the protein sequence modified according to the datasheet of purchased S protein. Peptide and protein assignments were by setting: trypsin as enzyme; three missed cleavages per peptide; mass tolerance of ± 50 ppm for precursor ions and ± 0.8 Da for fragment ions. Each condition/sample was run in LC-MS twice for technical replications (N runs = 6).

2.6. Computational methods

Both the structure with three-RBD-down (down) and one-RBD-up (up) of SARS-CoV-2 S protein were studied. The down conformation model 6vxx_1_2_1 (1–1146 AAs) without glycans, was taken from the CHARMM-GUI website (http://www.charmm-gui.org/docs/archive/covid-19, accessed on 10 June 2021), meanwhile the up model with glycans was taken from the last frame of 2 μs of classic MD simulation of the model N234-Man9_Replica1.pdb[29].

In order to model the UV^+ S protein both models have the disulphide bond broken, between Cys 1032 and Cys 1043 in all three chains.

MD simulations were performed using Amber 20 package [30], the ff14SB force field parameters was used for protein, meanwhile the GLYCAM06j-1 version of the GLYCAM06 force field was used for the glycans. Each complex was solvated in a periodic cubic water box using the TIP3P water model with 12 Å between the solutes and the edges of the box, then a suitable number of Na^+ and Cl^- ions were added to

neutralize the whole system. Each system was minimized in 6 consecutive minimization steps, each step of minimization was executed by the steepest descent method (15,000 steps) with decreasing positional restraints from 10 to 0 kcal/mol A^2 for each protein heavy atom. Other two consecutive minimization steps were executed, both composed by the steepest descent method (10,000 steps) followed by the conjugate gradient method (5000 steps). The systems were then subjected to two consecutive steps of heating, each of 500 ps, from 0.1 to 100 K and from 100 to 300 K with positional restraints for each protein heavy atom of 5 kcal/mol A^2, in an NVT ensemble with a Langevin thermostat. Bonds involving hydrogen atoms were constrained with the SHAKE algorithm and a 2 fs time step was used. The Van der Waals interactions were truncated at 11 Å and Particle Mesh Ewald (PME) was used to treat long-range electrostatics with B-spline interpolation of order 4. Then, the system was brought to 300 K an equilibration phase in the NPT ensemble of 1 ns and was used to set the pressure to 1 atm. The pressure was held constant with isotropic pressure scaling and a pressure relaxation time of 2.0 ps. At this point all restraints on the protein heavy atoms were removed, allowing the system to evolve for 15 ns of conformational equilibration and a classic MD for 150 ns of production in the down models (UV^- and UV^+ S) and 500 ns for the up models (UV^- and UV^+ S) were performed. Gaussian accelerated MD (GaMD) pmemd.cuda implementation from Amber 20 [31] was used to generate 2 μs for the down models (UV^- and UV^+ S) and 1.75 μs for the up models (UV^- and UV^+ S). The dual boost method was employed, adding a biasing force to both the total and dihedral potential energy. The threshold energy was set to the lower bound. GaMD production of equilibrated systems was carried out in five stages. In the first one, 10 ns of preparatory conventional MD simulation was carried out, without any statistics collected. In the second one, 20 ns of conventional MD was carried out to collect potential statistics Vmax, Vmin, Vavg, and σV. In the third one, 8 ns of GaMD was carried out with a boost potential applied with fixed parameters. Then, 80 ns of GaMD was carried out with updated boost parameters, and finally, the GaMD production run reported before was carried out with fixed boost parameters. All production simulations were carried out using the same parameters of the classic MD simulations.

The molecular dynamics simulations were carried out on the EOSC Compute Platform, a distributed federated compute infrastructure that serves users of the European Open Science Cloud (EOSC). The simulations were performed and analyzed using the tool Amber 20 on six virtual machines equipped with a total of 8 GPUs. As for the GPUs, dynamics were performed on devices based on the NVIDIA Ampere architecture. Specifically, four A100 GPUs that achieved a performance of approximately 35 ns/day, and four A40 GPUs that achieved a performance of approximately 26 ns/day. MD trajectories were analyzed using CPPTRAJ from AmberTools20 [30], and molecular graphics analysis was performed using the python package matplotlib [32], Visual Molecular Dynamics (VMD) [33] and Chimera X [34]. Root mean square deviations (RMSD) were calculated for all C-alpha atoms of the individual S chains and for the entire system. Furthermore, the conformational ensembles obtained from GaMD production runs of the trajectory, in which the RMSD values were stable along the trajectory, were used to compute the RMSF of C-alpha atoms and for clustering analysis using the hierarchical agglomerative (bottom-up) approach with epsilon 2.0 on 720–729,1026–1068 AAs. Hydrogen bonds analysis was carried out along trajectories obtaining the hydrogen bond frequency for each residue pair and the results were visualized on the representative structures by Chimera X. Essential dynamics (ED) analysis was performed using Principal Component Analysis (PCA) on each trajectory. The principal modes of motion were visualized using VMD. The first normalized eigenvectors for RBD of UV^- and UV^+ were plotted along the trajectory, and the porcupine plot was used to visualize the direction of motion. Dynamic Cross Correlation analysis was obtained by the matrix corell command in CPPTRAJ and from the matrix the lines corresponding to the Cys1032 and Cys1043 for each chain were selected for visualization.

2.7. Surface plasmon resonance (SPR) analysis

A BIAcore X-100 instrument (GE-Healthcare) was used. ACE2 was immobilized on one of the two flow cells of a CM5 sensor chip by standard amine-coupling chemistry as previously described[35]. On the second flow cell, BSA was immobilized to be used for blank subtraction. Different sensor-chips were prepared and used for the analyses, with the amount of immobilized ACE2 and BSA ranging from 2400 to 7300 RU (equal to 19–58 femtomoles/mm^2), and 1600 to 13,300 RU (equal to 22–186 femtomoles/mm^2), respectively. To compare the capacity of UV^- and UV^+ S to bind ACE2, the S protein was injected over the sensorchip at increasing concentration in HBS-EP buffer (0.01 M HEPES pH 7.4, 0.15 M NaCl, 3 mM EDTA, 0.005% v/v Surfactant P20) by adopting the single cycle model [36]. Dissociation Constant (Kd) values were calculated by steady state analyses performed by fitting the proper form of Scatchard's equation for the plot of the bound resonance units (RU) at equilibrium *versus* the compound concentration in solution.

2.8. Statistical analyses

Validation of identified peptides was performed in Proteome Discoverer 2.1 by Target Decoy PSM Validator and a false discovery rate (FDR) ≤ 0.01 (strict) and FDR ≤ 0.05 (relaxed) and maximum deltaCN of 0.05. The minimum peptide length of 4 amino acids at confidence medium level was set.

For the study variables, medians and ranges were reported for quantitative variables, and absolute and relative frequencies were reported for categorical variables. The Student's *t*-test and analysis of variance (ANOVA) were applied when appropriate. A p-value < 0.05 was set as cutoff for significance, for both SPR and nLC-MS analyses, also. Data were expressed as mean ± SEM.The analyses were performed using GraphPad Prism 9.

3. Results

As a proof of concept of our multidisciplinary approach, the effect of low UV-C (273 nm) irradiation on SARS-CoV-2 S protein was investigated by coupling preliminary *in vitro* infection assay, mass spectrometry (MS), protein 3D modelling and surface plasma resonance (SPR), to evaluate UV-irradiation effect on S.

3.1. UV-C irradiation at different irradiance/time combinations

Results indicated that a 4 mJ/cm^2 UV-C dose at 273 nm is capable of completely inhibiting viral replication. This outcome confirms and adds to our previous results documenting the antiviral effect of UV-C at 253 nm and 278 nm [17,21]. Importantly, the present results indicate that virus inhibition is dependent on the total irradiation dose alone, regardless of the time required to provide such dose, at least in the range used (a factor 20 in irradiance/time). In other words, virus inactivation relies exclusively on the total photons delivered to the sample, and such inhibition is maintained over time, as assessed by monitoring SARS-CoV-2 replication both in the cell supernatants (Fig. 2A and B) and at intracellular level at 7 days post infection (dpi) (Fig. 2C).

3.2. Mass spectrometry (MS) investigation of UV-C-induced S protein modifications

The UV-C light effects on S protein were assessed through high-resolution MS coupled to nano-liquid chromatography (nLC-MS) to characterize modifications on tryptic peptides.

These analyses allowed a total sequence coverage of nearly 76% for the S protein. Of note, nLC-MS analyses presented a poor coverage in the range of 529-to-733 aminoacids (AAs), which represents the proximity region between S1 and S2 domain (S1 domain: 13–685 AAs; S2 domain: 686–1273 AAs; S2/S2': 686–816 AAs), due to the low number of tryptic

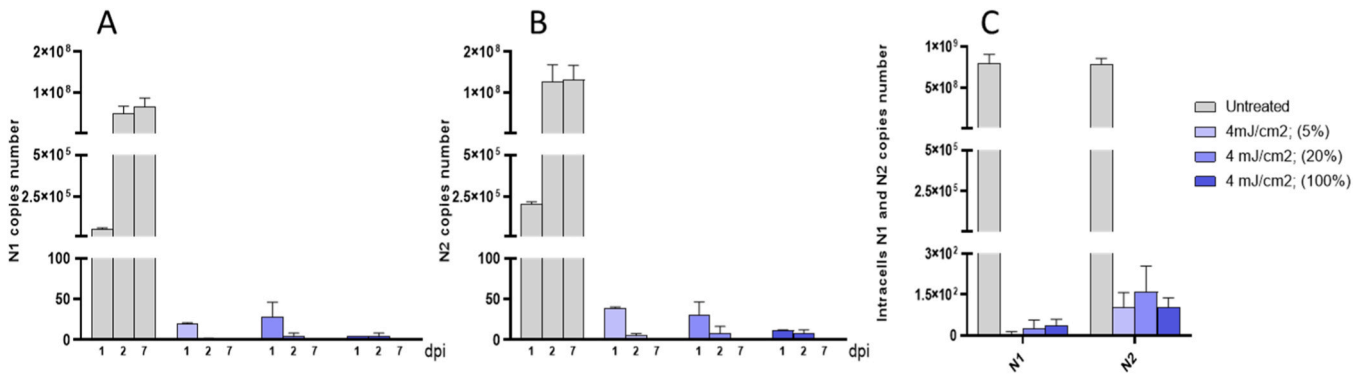

Fig. 2. Viral replication of UV-C-irradiated SARS-CoV-2 in *in vitro* infection assay. VeroE6 cells were infected with UV^- and UV^+ SARS-CoV-2 (1.5×10^3 $TCID_{50}$). The virus was irradiated using different UV-C irradiances (5, 20, 100%) and by adapting time of exposure in order to obtain 4 mJ/cm^2. Cell culture supernatants were harvested at the indicated times (1, 2 and 7 dpi) and virus titers were measured by absolute copy number quantification (Real-Time PCR) targeting viral genes N1 (A) and N2 (B). Viral load was assessed even on cell lysates harvested at the end of cell cultures (7 dpi) (**C**). For each condition, cells were seeded in duplicate. Mean values ± SEM from 3 experiments are shown.

sites (lysine, K, or arginine, R); instead, the Receptor Binding Domain (RBD) domain (319–541 AAs), as well as the N- and C-termini were almost completely covered by proteomic analysis (Figs. 3 and S1).

The structure of peptides from UV^+ and UV^- S protein was compared to verify which of them was modified by UV-C irradiation. As reported by Zhang et al., 2022 [37], the light-induced post-translational modifications (PTMs) potentially include: oxidation, dehydration, hydration, deamination, as well as cysteine (Cys) oxidation in sulfinic and sulfonic acids, which were all investigated in the present study (Table S1).

Based on repeatability and statistical confidence, three peptides were selected for further evaluation. Two of them, GVYYPDK (35–41 AAs), GIYQTSNFR (311–319 AAs) are localized on the S1 domain, and the third one MSECVLGQSKRVDFCGK (1029–1045 AAs) on the S2 domain.

Following UV-C irradiation, the two peptides on S1 changed in abundance (Fig. 4A and B), but no PTMs were detected. These findings might be correlated to an electron rearrangement followed by a folding variation, potentially determining a different exposition of tryptic site on the S protein (see computational evaluation reported below).

As for the MSECVLGQSKRVDFCGK peptide on S2 (Figs. 4C and S2), UV-C irradiation resulted in the oxidation in one of the cysteines, disrupting the disulphide bond Cys1032-Cys1043. Of note, this disulphide bridge is located in a conserved structural region of the trimeric S protein; as such, it was further characterized on 3D protein modelling.

Finally, based on MS data, single synthetic peptides corresponding to the three selected sequences altered by UV treatment (29-TNSFTRGVYYPDKVFRS-45; 309-EKGIYQTSNFRVQPTES-325; 1030-SECVLGQSKRVDFCGKG-1046), as well as a mixed synthetic peptide library of the whole S protein were irradiated with UV-C, and potential modifications were searched by nLC-MS, compared to untreated ones. No variations were detected (data not shown), indicating that UV-C-induced modifications are evident only on the folded and entire protein.

3.3. Structural and dynamic effects on S protein after UV-C exposition

Previous sequence analysis and structural comparison among spike proteins (MERS-CoV, SARS-CoV and SARS-CoV-2), show that Cys1032 and Cys1043, which were identified in the present study by MS, are located in the S2 subunit of the S protein, close to a region of highly preserved residues that are involved in the formation of a prominent H-bond cluster (Fig. 5) [38]. To assess the role played by the Cys1032-Cys1043 disulphide bond in the structure and function of the S protein, molecular dynamics (MD) simulations were performed for the UV^- trimeric form, and for UV^+ that has the broken disulphide bond in open (up) and closed (down) conformations. The root mean square deviation (RMSD) values were calculated among the initial conformation of S structure and all the following conformations to verify the stability of the systems; as shown in Fig. S3, all systems are well equilibrated. Analysis of the MD trajectories show that after UV-C treatment, the central network of H-bonds is ruptured in both conformations, the open and closed one (Fig. 5).

To explore the effect of the breaking disulphide bridge in the UV^+ structure and dynamics, the root mean square fluctuations (RMSF) of each residue was calculated; the difference between the RMSF values of the UV^+ and UV^- S protein for each chain, is shown in Fig. S4A. Regions with the greatest difference in the RMSF values between the UV^+ and the UV^- are in the receptor binding motif (RBM) region, which interacts directly with the human Angiotensin-Converting Enzyme 2 (ACE2) receptor, and in the NTD domain.

To understand how the local disruption of the H-bond cluster, close to Cys1032 and Cys1043, affects the dynamic behaviour of S protein potentially altering the affinity for the ACE2 receptor, the long-range protein correlated motion was investigated. Indeed, correlative and anti-correlative motions play a vital role in recognition and binding in a biological-complex system, and they can be extrapolated from MD simulation trajectory [39].

The difference between the dynamic cross-correlation coefficients of the UV^- and UV^+ S protein in up conformation were computed. From the complete dynamic cross-correlation map, showing for each residue those ones correlated with its motion, only the correlations of the cysteines belonging to the disulphide bond were reported in Fig. S4B.

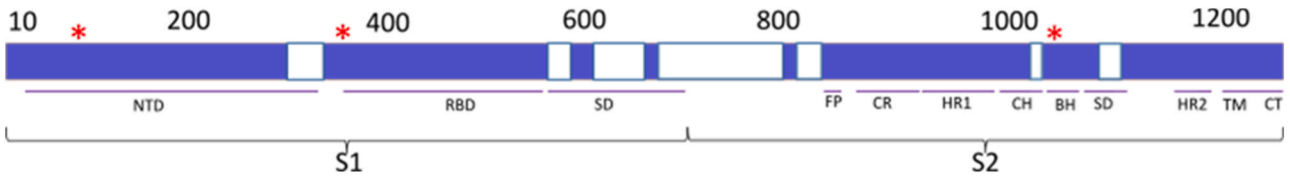

Fig. 3. S protein coverage obtained by nLC-MS analysis. Covered and uncovered sequences are reported as colourful and blank boxes, respectively. NTD= N-terminal domain, RBD= receptor-binding domain, SD= subdomain, FP= fusion peptide, CR: connecting region, HR1 = heptad repeat 1, CH= central helix, BH= β-hairpin, HR2 = heptad repeat 2, TM= transmembrane domain, CT= cytoplasmic tail. The positions of the three selected peptides are indicated by a red asterisk (*).

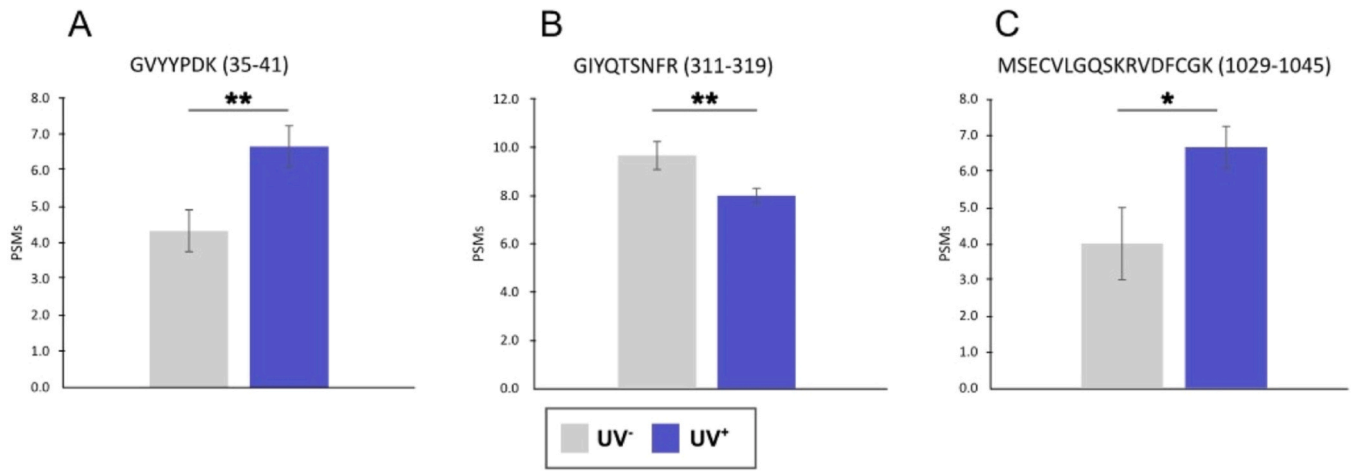

Fig. 4. Quantification of selected peptides by nLC-MS analysis. Selected peptides are quantified before and after UV-C irradiation using Peptide Matches (PSMs) values for UV^-(grey) and UV^+ (blue). (A) GVYYPDK, (B) GIYQTSNFR, (C) MSECVLGQSKRVDFCGK. * $p < 0.05$; * *p < 0.01.

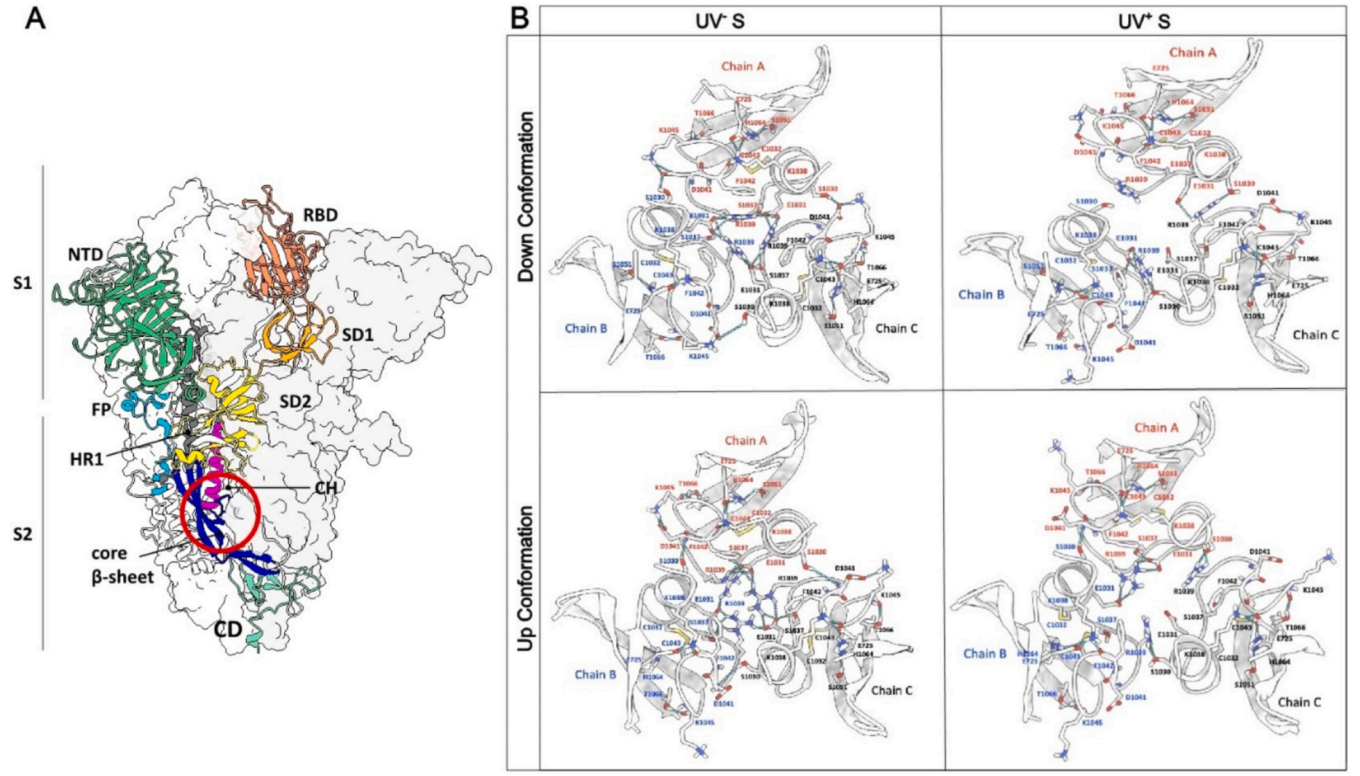

Fig. 5. MD trajectories. (A) Schematic representation of the SARS-CoV-2 S1-S2 protein structure. One of the three S chains is shown in the cartoon and coloured according to its domains: NTD in green, RBD in orange, SD1 bright orange, SD2 in yellow composing the S1 subunit and FP in cyan, HR1 in grey, CH in pink, core β sheet in blue and CD in light green composing the S2 subunit. (B), The up- and down-conformations of UV^+ and UV^- S local structures (res 720–729,1026–1068) near the Cys1032-Cys1043 disulphide bridge are depicted as cartoons; residues involved in the central H-bond network are shown as sticks coloured by chain A (red), chain B (blue) and chain C (black). H-bonds are shown as cyan dotted lines.

Data indicate that the breaking of the disulphide bond generates a long-distance correlated motion from the S2 to the S1 subunit, as further confirmed by the RMSF difference of regions as shown in Fig. S4A. This long-distance correlation may indeed be caused by a cumulative effect of many small local fluctuations on the way toward the RBD, along structural patches connecting these sites, allowing "distant" residues like Cys1032 and Cys1043 to affect RBD domain functionality.

Checking the extreme movements of the C-alpha atoms in the S1subunit, we observed that the UV^+ RBD in open conformation moves inward the center of the protein (Fig. 6). This results in a closer conformation altering the binding region to the cellular receptor, although the overall form of the S protein is mostly unchanged.

3.4. Effect of UV-C treatment on the capacity of S protein to bind to ACE-2

To assess whether UV-C-induced modifications alter the capacity of the S protein to bind to ACE2, UV^- and UV^+ S proteins were subjected to SPR binding analysis onto a biosensor containing immobilized ACE2. As shown in Fig. 7A, injection of increasing concentrations of the two forms

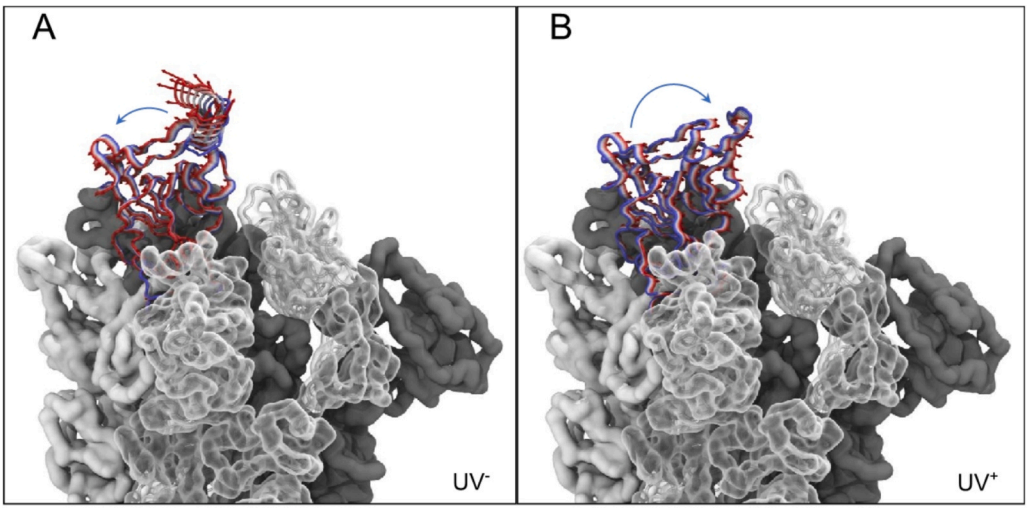

Fig. 6. Extreme movements of the C-alpha atoms of the S1 domain along the first principal component. Change in motion of the up-RBD is shown in cartoon by the superimposition of ten conformations extracted at equal time intervals along the trajectories (from blue to red) and projected onto the first essential dynamics eigenvector for the UV^- (A) and UV^+ (B). The porcupine plot corresponding to C-alpha atom projections of the RBD domain onto the first normal mode is shown as well.

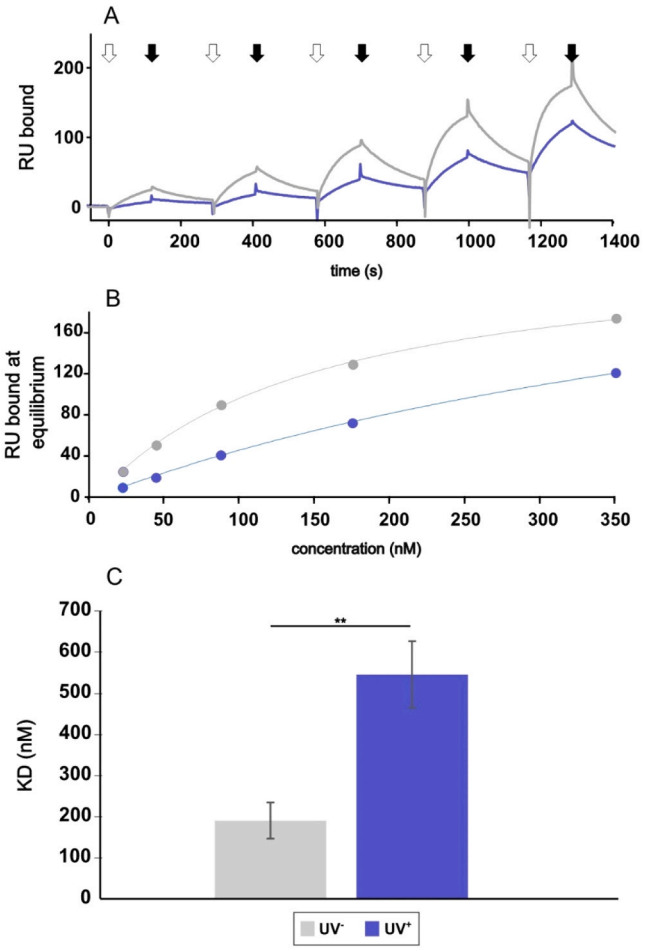

Fig. 7. SPR analysis of the UV^- or UV^+ S protein binding to sensorchip-immobilized ACE2. (A) Overlay of blank-subtracted sensorgrams derived from a single cycle analysis of UV^- (gray) or UV^+ (blue) S proteins at 9.4, 18.8, 40, 37.5, 75, 150 mM injected on the ACE2 biosensor. White and black arrows point to the start and end of the injections, respectively. (B) Overlay of the steady-state analysis of UV^- (gray) or UV^+ S (blue) injected onto the ACE2 biosensor. The results shown are representative of three n = 3 experiments that gave similar results. (C) Kd of the UV^- or UV^+ S protein interaction with sensorchip-immobilized ACE2. The difference between the calculated Kd mean value is statistically significant (** $p < 0.006$).

of S protein onto the ACE2-containing biosensor provided saturable and dose-dependent sensorgrams. Saturation curves could be plotted with the binding values at equilibrium (Fig. 7B), allowing the calculation of the dissociation constant (Kd) value, that is inversely proportional to the binding affinity. As shown in Fig. 7C, UV-C exposure causes a significant 3-fold decrease of the S protein binding affinity to ACE2. These data, in line with those provided by the modelling analyses, suggest that UV-C irradiation significantly impairs S protein interaction with ACE2, thus hampering virus infectivity, as supported by the *in vitro* infection assays.

4. Discussion

The ultimate goal of virus–host protein interaction studies is to dissect interaction events that are critical for different stages of a viral infection, and could serve as molecular targets for the formulation of new pharmaceutical approaches. In this setting, the integration of proteomics approach to virology has enabled a significant coverage of biological insight into the mechanisms of virus-host protein-protein interactions driving cellular infection. In particular, the application of nLC-MS analyses has allowed high-throughput profiling of viral protein domains/sequences involved in the host-infection process [40,41].

Likewise, computational analyses and interpretation of the bioinformatic datasets allow for the assessment of interaction specificity, and the generation of virus–host protein interaction networks [42].

To date, these advances in proteomic and computational methods have paved the way for the identification of an impressive number of virus–host protein associations that might not have been otherwise uncovered by more traditional approaches. However, the independent use of these methodologies provides only a partial, non-exhaustive overview.

The workflow developed through the present study integrates the expertise of different scientific teams to offer a successively detailed analysis from the macroscopic to the molecular perspective: virus, protein, domain, peptide, aminoacids. As a result, the pipeline here presented enables identification and molecular characterization of those pathogen domains that are mostly susceptible to alterations induced by a wide variety of biophysical, biochemical, or pharmacological approaches. Focusing on structural proteins with a key role in the cell-internalization step enables in-depth characterization of the pathogen-host interactions and allows for the identification of specific subunits serving as potential therapeutic targets.

Briefly, the workflow provides a preliminary phase that involves exposure of the microorganism to a specific treatment/compound that is either known or expected to interfere with its life-cycle as assessed by monitoring through an *in vitro* infection assay aver time. Once the latter

has been established, it is possible to investigate the causes behind this phenomenon through a focused analysis on the microbial domains that are mostly susceptible to treatment-induced alterations. In detail, the next in-depth investigation consists of three different, but complementary approaches aimed at: i) characterizing the pathogen ligand - host receptor binding affinity (SPR), ii) identifying altered levels of peptides after treatment/exposure (nLC-MS) and iii) evaluating the effect of treatment-induced alteration on the protein structure and therefore the protein loss/gain of function (Computational methods).

In our pilot study model, we employed UV-C radiation based on its previously established microbicidal efficacy against a wide range of viral species, including SARS-CoV-2 [21,43–48]. This occurs primarily by damaging viral nucleic acids. However, our intent was to exploit the effect of UV radiation upon viral proteins (capsid/receptors) which are involved in the recognition of target host cells and absorb in the same spectral range [18,19], so as to identify any alterations which could disclose susceptible molecular domains. Pioneering studies [17,21] assessing the minimum UV-C-dose necessary to completely inactivate SARS-CoV-2, showed that a 4 mJ/cm^2 dose almost abrogates viral infectivity. Herein, by adopting the multidisciplinary approach, we investigated the effect of low UV-C irradiation (273 nm) on SARS-CoV-2 S protein, as in our hands, treatment with this UV wavelength is sufficient to hamper SARS-CoV-2 infectivity, as documented by fluorescence *in situ* hybridization (FISH) [17].

The S protein consists of two subunits, namely S1 and S2. The S1 subunit contains the RBD, which mediates virus binding to the ACE2 receptor. Conversely, the S2 subunit, which includes a fusion peptide (FP), the heptad repeat (HR) 1 and 2, transmembrane (TM) and cytoplasmic fusion (CT) domains, regulates viral-cell membrane fusion by forming a six-helical bundle *via* the two-HR domains [49]. To verify whether UV-C exposure modifies the S protein, and specific AAs, we coupled MS to molecular modelling and receptor binding affinity analyses.

Label-free MS-based results showed that several reproducible AA modifications occur in the S protein following UV-C irradiation. Among these, we focused on a peptide sequence (MSECVLGQSKRVDFCGK) within the S2 domain in an internal site of the tri-dimensional protein conformation. Notably, the MSECVLGQSKRVDFCGK peptide contains a disulphide bridge, which is partially disrupted and oxidized following UV-C irradiation. This appears particularly relevant when considering that the 14 disulphide bonds within the S protein [49,50] are crucial to stabilize the tertiary and quaternary protein conformation, as well as to preserve its flexibility and dynamicity. These features are essential to guarantee its conformational transitions, as the S protein must shift from an inactive “down” position to an active “up” one in order to properly accomplish the two-step infection process [51]. The key function displayed by these bridges is further endorsed by evidence that mutations of these Cys residues result in either a significant decrease in the expression levels or a complete loss of function [52].

As for the effect of UV-C irradiation, it has already been reported that the structural integrity of any disulphide bonds may be compromised due to the high vibrational excitation energy related to high-lying Rydberg states [53]. Normally, this vibrational energy occurs in few aromatic AAs inside the peptide that promote the energy transfer to Cys-Cys bond, thus causing photodissociation breakage/cleavage [54,55]. Notably, each of the two (GVYYPDK and GIYQTSNFR) out of the three selected peptides contains 2 aromatic AAs. UV-C disulphide bridge disruption on the RBD domain was recently investigated by Shi et al. [56] by means of reducing agents and MS-based approach. By using non-cytotoxic thiol-based chemical probes, the authors concluded that the UV-C antiviral activity is based on redox mechanisms disrupting the RBD disulphides. Moreover, molecular dynamics simulation analyses underlined the critical impact of conformational changes in the RBD motif occurring concomitantly with breakage of Cys-Cys disulphide pairs, despite their distance to the ACE2 recognition motif [56].

Our results show that UV-C-related disruption of disulphide bonds occurs within the S2 domain rather than the RBD, possibly impairing the protein’s dynamic, which in turn, may affect the virus ability to enter host cells. In this scenario, our computational analysis shows that the UV-C-induced Cys1032-Cys1043 disruption destabilizes the local hydrogen bond network, causing internal fluctuations of the AA residues from the S2 to the S1 subunit. This long-range allosteric effect in turn triggers inward movements of the RBD, fostering a closer conformation which is less prone to bind the ACE2 receptor. This speculation would also explain why the isolated synthetic peptides corresponding to the identified regions, and the whole synthetic library of overlapping peptides were not affected by UV-C treatment. Only the maintenance of the overall 3D S protein structure would allow the disulphide bridge to act as a quencher of the aromatic chromophore excited states and the propagation of the disruptive UV-C effect from the S2 to the S1 domain, hampering its binding to ACE2. This is actually confirmed by SPR binding analysis that demonstrated a significant 3-fold reduction of the binding affinity of the S protein to its ACE2 receptor after UV irradiation.

Further endorsing this speculation, a similar phenomenon has been previously observed for the SARS-CoV S protein. Indeed, mutations of two conserved Cys residues, forming a disulphide bridge in the S2 domain, led to a reduction of membrane fusion capability compared to the wild type one, which was even more striking when a double mutant was analysed [57]. Results herein are likely to be far more important considering that the identified sequence in the S2 domain of SARS-CoV-2 is crucial to determining the integrity of the binomial structural-functional role of the S protein. Recent studies [58,59] systematically examining functional dynamics and regulatory centers of S trimer, showed that the SARS-CoV-2 S protein acts as an allosteric regulatory engine that fluctuates between dynamically distinct functional states.

Remarkably, a stabilizing structural role has been assigned to the S2 subunit acting as an anchoring region for the signal transmission in the S protein; this suggests that allosteric signaling mechanisms may be governed by functional regions in the β-sheet core and CH regions, where the identified disulphide bridge is located [60]. Such domains are highly conserved among different coronaviruses [61], supporting their relevance in the maintenance of the S glycoprotein structure. Indeed, the degree of evolutionary conservation of AA residues is often a suggestion of their functional significance [62].

We wish to point out that the present study is not devoid of limitations. Traditional reduction and alkylation protocols are used in proteomics investigations to improve the coverage of sequences, preventing the shuffling of S-S bridge. However, as these procedures produce artifacts, the experimental investigation of protein structure herein adopted implies the need to avoid reduction and alkylation in order to characterize the actual disulphide bridge status. Alternatively, digestion by enzymes working at pH < 4, such as pepsin might be applied [63]; however, besides lacking digestion specificity, controlling its activity is challenging. Also, the conformational change observed in the computational analysis needs to be validated by sophisticated procedures, such as using hydrogen–deuterium exchange [40] or more complex cross-linking protocols [64,65] to study interaction with ACE2.

Another potential limitation of our approach is that it identifies potential targets but gives no specific hints on effector molecules on these targets, which on the one hand, implies the need of coupling it with additional targeted analyses such as high throughput screenings. On the other hand, high-throughput screening of small molecules selects some hits but for their optimization, a knowledge of their mechanism of action is required. Again, a major drawback of high throughput screenings is the chance of false positives, as it leads to a high failure rate between the number of hits and the number of authentic lead compounds, which must be eliminated early. In this frame, our approach can be complementary to high throughput screening by aiding in the identification and elimination of false positives, or even in improving its efficiency and effectiveness by focusing the analyses on a limited number of relevant targets. In this case, we suggest reducing agents as potential effector

molecules, but only drug discovery studies could identify specific and selective molecules able to break the disulphide bridge that we have identified.

These limits notwithstanding, the proposed multidisciplinary approach allows a preliminary screening useful to characterize potential domains modified by UV-C irradiation. This approach, although it took time and resources, elucidated a key inhibitory mechanism of SARS-CoV-2 entry. The proposed model identifies the S2' subunit of the S protein as a novel and potential target for developing new antiviral treatments, such as thiol-reducing compounds, to be applied in pre-clinical practices. Indeed, although the S protein has attracted huge interest in vaccine/therapeutic drug discovery, the high variability of the S1/RBD domain has drastically hindered the possibility to target it with broad-spectrum antiviral inhibitors [61]; conversely, the recently highlighted benefits of employing S2' over S1' in vaccines and potential therapies [66] suggest the possibility to pharmacologically exploit it. Advantages include extant cross-reactive neutralizing antibodies in populations (due to prior exposure to common cold coronaviruses), the steric neutralization potential of antibodies against S2, and the stronger memory B-cell and T-cell elicited responses and most importantly, the structural conservation of S2 [66,67], as recently occurred for conserved regions of other viruses [68]. Our approach has shown that a physical inactivator such as UV-C radiation destroys an S2' disulphide bond, which could be exploited for targeting chemical probes that act as reducing agents to inhibit infection by SARS-CoV-2 and decrease the binding of S glycoprotein to its receptor ACE2. Our findings represent a starting point for the characterization of the functional groups of chemical inactivators, a fundamental information for the implementation of a ligand library to be used in virtual screening approaches. These concepts further emphasize the need for an in-depth characterization of the structural, and molecular accessibility and stability of S2' in the frame of SARS-CoV-2 prevention and treatment. More broadly, we do expect to take advantage from the roadmap fine-tuned in this study to screen molecular domains of other pathogens resulting in a precise molecular fingerprint and providing new insights to adequately address future epidemics.

Funding

Partially supported by Fondazione Alessandro e Vincenzo Negroni e Fondazione Romeo ed Enrica Invernizzi. PON R&I PIR01_00017 Centro Nazionale di Ricerca in Bioinformatica per le Scienze "OMICHE" – CNRBIOMICS, ELIXIRxNextGenIT [PNRR, Prot. IR0000010] and Telethon-Cariplo project 3833, lmplementation Study- Proteomics 2019–2021, ELIXIR Europe Consortium, towards PLM; EGI-ACE Horizon 2020 project that granted access to EOSC infrastructure, D'U.P. BBMRI. it (Italian national node of BBMRI-ERIC), a research infrastructure financed by the Italian Government and by the Italian Ministry of University and Research through the "Strengthening of the Biobanking and Biomolecular Resources Research Infrastructure of Italy" project (PNRR IR0000031) to AM. This research was also supported by EU funding within the NextGenerationEU-MUR PNRR Extended Partnership initiative on Emerging Infectious Diseases (Project no. PE00000007, INF-ACT)

CRediT authorship contribution statement

Sergio Strizzi: Methodology, Investigation, Writing – original draft. **Letizia Bernardo**: Methodology, Investigation, Writing – review & editing. **Pasqualina D'Ursi**: Methodology, Investigation, Writing – original draft, Writing – review & editing. **Chiara Urbinati**: Investigation. **Andrea Bianco**: Conceptualization. **Fiona Limanaqi**: Methodology, Investigation, Investigation, Writing – review & editing. **Andrea Manconi**: Software. **Maria Milanesi**: Methodology, Investigation, Writing – original draft. **Alberto Macchi**: Methodology, Investigation. **Dario Di Silvestre**: Methodology, Software. **Adalberto Cavalleri**: Conceptualization. **Giovanni Pareschi**: Conceptualization. **Marco Rusnati**: Methodology, Writing – review & editing. **Mario Clerici**: Funding acquisition, Writing – review & editing. **PierLuigi Mauri**: Conceptualization, Funding acquisition, Project administration, Supervision, Writing – original draft. **Mara Biasin:** Conceptualization, Funding acquisition, Project administration, Supervision, Writing – original draft, Writing – review & editing.

Declaration of Competing Interest

The authors declare that they have no known competing financial interests or personal relationships that could have appeared to influence the work reported in this paper.

Data availability

Data will be made available on request.

Acknowledgments

We acknowledge BEI Resources NIAID, NIH (Manassas, VA, USA) for providing the Peptide Array, SARS-Related Coronavirus 2S Glycoprotein for free.

Data and materials availability

All raw data supporting the conclusions of this article will be made available by the authors, without undue reservation. The proteomic datasets (in form of raw data) analyzed for this study can be found in the MassIVE database at the site: [massive.ucsd.edu] at link ftp://massive.ucsd.edu/MSV000090915/.

Appendix A. Supporting information

Supplementary data associated with this article can be found in the online version at doi:10.1016/j.phrs.2023.106862.

References

[1] K.R. Wigginton, T. Kohn, Virus disinfection mechanisms: the role of virus composition, structure, and function, Curr. Opin. Virol. 2 (2012) 84–89, https://doi.org/10.1016/j.coviro.2011.11.003.
[2] Y. Zhang, J. Wei, Y. Qiu, C. Niu, Z. Song, Y. Yuan, T. Yue, Structure-Dependent Inhibition of Stenotrophomonas maltophilia by Polyphenol and Its Impact on Cell Membrane, Front. Microbiol. 10 (2019) 2646, https://doi.org/10.3389/fmicb.2019.02646.
[3] Q. Wang, F. Meng, Y. Xie, W. Wang, Y. Meng, L. Li, T. Liu, J. Qi, X. Ni, S. Zheng, J. Huang, N. Huang, In silico discovery of small molecule modulators targeting the achilles' heel of SARS-CoV-2 Spike Protein, ACS Cent. Sci. (2023), https://doi.org/10.1021/acscentsci.2c01190 acscentsci.2c01190.
[4] C. Wu, Y. Liu, Y. Yang, P. Zhang, W. Zhong, Y. Wang, Q. Wang, Y. Xu, M. Li, X. Li, M. Zheng, L. Chen, H. Li, Analysis of therapeutic targets for SARS-CoV-2 and discovery of potential drugs by computational methods, Acta Pharm. Sin. B 10 (2020) 766–788, https://doi.org/10.1016/j.apsb.2020.02.008.
[5] J. Geddes-McAlister, N. Prudhomme, D. Gutierrez Gongora, D. Cossar, M. D. McLean, The emerging role of mass spectrometry-based proteomics in molecular pharming practices, Curr. Opin. Chem. Biol. 68 (2022), 102133, https://doi.org/10.1016/j.cbpa.2022.102133.
[6] J. Shang, Y. Wan, C. Luo, G. Ye, Q. Geng, A. Auerbach, F. Li, Cell entry mechanisms of SARS-CoV-2, Proc. Natl. Acad. Sci. U.S.A. 117 (2020) 11727–11734. https://doi.org/10.1073/pnas.2003138117.
[7] L. Du, Y. He, Y. Zhou, S. Liu, B.-J. Zheng, S. Jiang, The spike protein of SARS-CoV — a target for vaccine and therapeutic development, Nat. Rev. Microbiol 7 (2009) 226–236, https://doi.org/10.1038/nrmicro2090.
[8] K. Stadler, H.R. Ha, V. Ciminale, C. Spirli, G. Saletti, M. Schiavon, D. Bruttomesso, L. Bigler, F. Follath, A. Pettenazzo, A. Baritussio, Amiodarone alters late endosomes and inhibits SARS coronavirus infection at a post-endosomal level, Am. J. Respir. Cell Mol. Biol. 39 (2008) 142–149, https://doi.org/10.1165/rcmb.2007-0217OC.
[9] L. Yi, Z. Li, K. Yuan, X. Qu, J. Chen, G. Wang, H. Zhang, H. Luo, L. Zhu, P. Jiang, L. Chen, Y. Shen, M. Luo, G. Zuo, J. Hu, D. Duan, Y. Nie, X. Shi, W. Wang, Y. Han, T. Li, Y. Liu, M. Ding, H. Deng, X. Xu, Small molecules blocking the entry of severe acute respiratory syndrome coronavirus into host cells, J. Virol. 78 (2004) 11334–11339, https://doi.org/10.1128/JVI.78.20.11334-11339.2004.

[10] I. Mahmud, T.J. Garrett, Mass spectrometry techniques in emerging pathogens studies: COVID-19 perspectives, J. Am. Soc. Mass Spectrom. 31 (2020) 2013–2024, https://doi.org/10.1021/jasms.0c00238.
[11] T.M. Greco, I.M. Cristea, Proteomics tracing the footsteps of infectious disease, Mol. Cell. Proteom. 16 (2017) S5–S14, https://doi.org/10.1074/mcp.O116.066001.
[12] J. Gillen, A. Nita-Lazar, Experimental analysis of viral–host interactions, Front. Physiol. 10 (2019) 425, https://doi.org/10.3389/fphys.2019.00425.
[13] Y. Luo, M.A. Muesing, Mass spectrometry-based proteomic approaches for discovery of HIV–host interactions, Future Virol. 9 (2014) 979–992, https://doi.org/10.2217/fvl.14.86.
[14] Y.-C. Lai, Y.-W. Cheng, C.-H. Chao, Y.-Y. Chang, C.-D. Chen, W.-J. Tsai, S. Wang, Y.-S. Lin, C.-P. Chang, W.-J. Chuang, L.-Y. Chen, Y.-R. Wang, S.-Y. Chang, W. Huang, J.-R. Wang, C.-K. Tseng, C.-K. Lin, Y.-C. Chuang, T.-M. Yeh, Antigenic Cross-Reactivity Between SARS-CoV-2 S1-RBD and Its Receptor ACE2, Front. Immunol. 13 (2022), 868724, https://doi.org/10.3389/fimmu.2022.868724.
[15] A.A.T. Naqvi, F. Anjum, A. Shafie, S. Badar, A.M. Elasbali, D.K. Yadav, Md. I. Hassan, Investigating host-virus interaction mechanism and phylogenetic analysis of viral proteins involved in the pathogenesis, PLoS ONE 16 (2021), e0261497, https://doi.org/10.1371/journal.pone.0261497.
[16] S. Thakur, S. Sasi, S.G. Pillai, A. Nag, D. Shukla, R. Singhal, S. Phalke, G.S.K. Velu, SARS-CoV-2 mutations and their impact on diagnostics, therapeutics and vaccines, Front. Med. 9 (2022), 815389, https://doi.org/10.3389/fmed.2022.815389.
[17] M. Biasin, S. Strizzi, A. Bianco, A. Macchi, O. Utyro, G. Pareschi, A. Loffreda, A. Cavalleri, M. Lualdi, D. Trabattoni, C. Tacchetti, D. Mazza, M. Clerici, UV and violet light can Neutralize SARS-CoV-2 Infectivity, J. Photochem. Photobiol. 10 (2022), 100107, https://doi.org/10.1016/j.jpap.2021.100107.
[18] L. Guo, R. Xu, L. Gou, Z. Liu, Y. Zhao, D. Liu, L. Zhang, H. Chen, M.G. Kong, Mechanism of virus inactivation by cold atmospheric-pressure plasma and plasma-activated water, Appl. Environ. Microbiol 84 (2018) e00726–18, https://doi.org/10.1128/AEM.00726-18.
[19] C. Zhang, Y. Li, D. Shuai, Y. Shen, D. Wang, Progress and challenges in photocatalytic disinfection of waterborne Viruses: A review to fill current knowledge gaps, Chem. Eng. J. 355 (2019) 399–415, https://doi.org/10.1016/j.cej.2018.08.158.
[20] K.A. Barrow, L.M. Rich, E.R. Vanderwall, S.R. Reeves, J.A. Rathe, M.P. White, J. S. Debley, Inactivation of Material from SARS-CoV-2-Infected Primary Airway Epithelial Cell Cultures, Methods Protoc. 4 (2021) 7, https://doi.org/10.3390/mps4010007.
[21] M. Biasin, A. Bianco, G. Pareschi, A. Cavalleri, C. Cavatorta, C. Fenizia, P. Galli, L. Lessio, M. Lualdi, E. Tombetti, A. Ambrosi, E.M.A. Redaelli, I. Saulle, D. Trabattoni, A. Zanutta, M. Clerici, UV-C irradiation is highly effective in inactivating SARS-CoV-2 replication, Sci. Rep. 11 (2021) 6260, https://doi.org/10.1038/s41598-021-85425-w.
[22] K.A. Reynolds, Integrated Cell Culture/PCR for Detection of Enteric Viruses in Environmental Samples, in: Public Health Microbiology, Humana Press, New Jersey, 2004: pp. 069–078. https://doi.org/10.1385/1–59259-766–1:069.
[23] F. Caccuri, A. Bugatti, A. Zani, A. De Palma, D. Di Silvestre, E. Manocha, F. Filippini, S. Messali, P. Chiodelli, G. Campisi, S. Fiorentini, F. Facchetti, P. Mauri, A. Caruso, SARS-CoV-2 infection remodels the phenotype and promotes angiogenesis of primary human lung endothelial cells, Microorganisms 9 (2021) 1438, https://doi.org/10.3390/microorganisms9071438.
[24] T. Nilsson, M. Mann, R. Aebersold, J.R. Yates, A. Bairoch, J.J.M. Bergeron, Mass spectrometry in high-throughput proteomics: ready for the big time, Nat. Methods 7 (2010) 681–685, https://doi.org/10.1038/nmeth0910-681.
[25] C. Procaccini, F. Carbone, D. Di Silvestre, F. Brambilla, V. De Rosa, M. Galgani, D. Faicchia, G. Marone, D. Tramontano, M. Corona, C. Alviggi, A. Porcellini, A. La Cava, P. Mauri, G. Matarese, The proteomic landscape of human ex vivo regulatory and conventional T cells reveals specific metabolic requirements, Immunity 44 (2016) 406–421, https://doi.org/10.1016/j.immuni.2016.01.028.
[26] L. Sereni, M.C. Castiello, D. Di Silvestre, P. Della Valle, C. Brombin, F. Ferrua, M. P. Cicalese, L. Pozzi, M. Migliavacca, M.E. Bernardo, C. Pignata, R. Farah, L. D. Notarangelo, N. Marcus, L. Cattaneo, M. Spinelli, S. Giannelli, M. Bosticardo, K. van Rossem, A. D'Angelo, A. Aiuti, P. Mauri, A. Villa, Lentiviral gene therapy corrects platelet phenotype and function in patients with Wiskott-Aldrich syndrome, J. Allergy Clin. Immunol. 144 (2019) 825–838, https://doi.org/10.1016/j.jaci.2019.03.012.
[27] C. Palma, C. La Rocca, V. Gigantino, G. Aquino, G. Piccaro, D. Di Silvestre, F. Brambilla, R. Rossi, F. Bonacina, M.T. Lepore, M. Audano, N. Mitro, G. Botti, S. Bruzzaniti, C. Fusco, C. Procaccini, V. De Rosa, M. Galgani, C. Alviggi, A. Puca, F. Grassi, T. Rezzonico-Jost, G.D. Norata, P. Mauri, M.G. Netea, P. de Candia, G. Matarese, Caloric Restriction Promotes Immunometabolic Reprogramming Leading to Protection from Tuberculosis, Cell Metabolism. 33 (2021) 300–318.e12. https://doi.org/10.1016/j.cmet.2020.12.016.
[28] D.L. Tabb, The SEQUEST family tree, J. Am. Soc. Mass Spectrom. 26 (2015) 1814–1819, https://doi.org/10.1007/s13361-015-1201-3.
[29] A.M. Harbison, C.A. Fogarty, T.K. Phung, A. Satheesan, B.L. Schulz, E. Fadda, Fine-tuning the spike: role of the nature and topology of the glycan shield in the structure and dynamics of the SARS-CoV-2 S, Chem. Sci. 13 (2022) 386–395, https://doi.org/10.1039/D1SC04832E.
[30] D.A. Case, H.M. Aktulga, K. Belfon, I.Y. Ben-Shalom, S.R. Brozell, D.S. Cerutti, T. E. Cheatham III, G.A. Cisneros, V.W.D. Cruzeiro, T.A. Darden, R.E. Duke, G. Giambasu, M.K. Gilson, H. Gohlke, A.W. Goetz, et al., AMBER 2020, University of California, San Francisco, CA, 2020.
[31] J. Wang, P.R. Arantes, A. Bhattarai, R.V. Hsu, S. Pawnikar, Y.M. Huang, G. Palermo, Y. Miao, Gaussian accelerated molecular dynamics: Principles and applications, WIREs Comput. Mol. Sci. 11 (2021), https://doi.org/10.1002/wcms.1521.
[32] J.D. Hunter, Matplotlib: A 2D Graphics Environment, Comput. Sci. Eng. 9 (2007) 90–95, https://doi.org/10.1109/MCSE.2007.55.
[33] W. Humphrey, A. Dalke, K. Schulten, VMD: Visual molecular dynamics, J. Mol. Graph. 14 (1996) 33–38, https://doi.org/10.1016/0263-7855(96)00018-5.
[34] E.F. Pettersen, T.D. Goddard, C.C. Huang, E.C. Meng, G.S. Couch, T.I. Croll, J. H. Morris, T.E. Ferrin, UCSF ChimeraX: Structure visualization for researchers, educators, and developers, Protein Sci. 30 (2021) 70–82, https://doi.org/10.1002/pro.3943.
[35] M. Rusnati, G. Paiardi, C. Tobia, C. Urbinati, A. Lodola, P. D'Ursi, M. Corrado, R. Castelli, R.C. Wade, M. Tognolini, P. Chiodelli, Cholenic acid derivative UniPR1331 impairs tumor angiogenesis via blockade of VEGF/VEGFR2 in addition to Eph/ephrin, Cancer Gene Ther. 29 (2022) 908–917, https://doi.org/10.1038/s41417-021-00379-5.
[36] H.-H. Trutnau, New multi-step kinetics using common affinity biosensors saves time and sample at full access to kinetics and concentration, J. Biotechnol. 124 (2006) 191–195, https://doi.org/10.1016/j.jbiotec.2006.01.006.
[37] Z. Zhang, S.-Y. Chow, R. De Guzman, N.H. Joh, M.K. Joubert, J. Richardson, B. Shah, M. Wikström, Z.S. Zhou, J. Wypych, A Mass Spectrometric Characterization of Light-Induced Modifications in Therapeutic Proteins, J. Pharm. Sci. 111 (2022) 1556–1564, https://doi.org/10.1016/j.xphs.2022.02.002.
[38] G.M. Verkhivker, L.Di Paola, Integrated Biophysical Modeling of the SARS-CoV-2 Spike Protein Binding and Allosteric Interactions with Antibodies, J. Phys. Chem. B 125 (2021) 4596–4619, https://doi.org/10.1021/acs.jpcb.1c00395.
[39] B.L. Kormos, A.M. Baranger, D.L. Beveridge, A study of collective atomic fluctuations and cooperativity in the U1A–RNA complex based on molecular dynamics simulations, J. Struct. Biol. 157 (2007) 500–513, https://doi.org/10.1016/j.jsb.2006.10.022.
[40] S.M. Costello, S.R. Shoemaker, H.T. Hobbs, A.W. Nguyen, C.-L. Hsieh, J. A. Maynard, J.S. McLellan, J.E. Pak, S. Marqusee, The SARS-CoV-2 spike reversibly samples an open-trimer conformation exposing novel epitopes, Nat. Struct. Mol. Biol. 29 (2022) 229–238, https://doi.org/10.1038/s41594-022-00735-5.
[41] M. Manček-Keber, I. Hafner-Bratkovič, D. Lainšček, M. Benčina, T. Govednik, S. Orehek, T. Plaper, V. Jazbec, V. Bergant, V. Grass, A. Pichlmair, R. Jerala, Disruption of disulfides within RBD of SARS-CoV-2 spike protein prevents fusion and represents a target for viral entry inhibition by registered drugs, FASEB J. 35 (2021), https://doi.org/10.1096/fj.202100560R.
[42] D.E. Gordon, G.M. Jang, M. Bouhaddou, J. Xu, K. Obernier, K.M. White, M.J. O'Meara, V.V. Rezelj, J.Z. Guo, D.L. Swaney, T.A. Tummino, R. Hüttenhain, R.M. Kaake, A.L. Richards, B. Tutuncuoglu, H. Foussard, J. Batra, K. Haas, M. Modak, M. Kim, P. Haas, B.J. Polacco, H. Braberg, J.M. Fabius, M. Eckhardt, M. Soucheray, M. J. Bennett, M. Cakir, M.J. McGregor, Q. Li, B. Meyer, F. Roesch, T. Vallet, A. Mac Kain, L. Miorin, E. Moreno, Z.Z.C. Naing, Y. Zhou, S. Peng, Y. Shi, Z. Zhang, W. Shen, I.T. Kirby, J.E. Melnyk, J.S. Chorba, K. Lou, S.A. Dai, I. Barrio-Hernandez, D. Memon, C. Hernandez-Armenta, J. Lyu, C.J.P. Mathy, T. Perica, K.B. Pilla, S.J. Ganesan, D.J. Saltzberg, R. Rakesh, X. Liu, S.B. Rosenthal, L. Calviello, S. Venkataramanan, J. Liboy-Lugo, Y. Lin, X.-P. Huang, Y. Liu, S.A. Wankowicz, M. Bohn, M. Safari, F.S. Ugur, C. Koh, N.S. Savar, Q.D. Tran, D. Shengjuler, S.J. Fletcher, M.C. O'Neal, Y. Cai, J.C.J. Chang, D.J. Broadhurst, S. Klippsten, P.P. Sharp, N.A. Wenzell, D. Kuzuoglu-Ozturk, H.-Y. Wang, R. Trenker, J.M. Young, D. A. Cavero, J. Hiatt, T.L. Roth, U. Rathore, A. Subramanian, J. Noack, M. Hubert, R. M. Stroud, A.D. Frankel, O.S. Rosenberg, K.A. Verba, D.A. Agard, M. Ott, M. Emerman, N. Jura, M. von Zastrow, E. Verdin, A. Ashworth, O. Schwartz, C. d'Enfert, S. Mukherjee, M. Jacobson, H.S. Malik, D.G. Fujimori, T. Ideker, C.S. Craik, S.N. Floor, J.S. Fraser, J.D. Gross, A. Sali, B.L. Roth, D. Ruggero, J. Taunton, T. Kortemme, P. Beltrao, M. Vignuzzi, A. García-Sastre, K.M. Shokat, B.K. Shoichet, N.J. Krogan, A SARS-CoV-2 protein interaction map reveals targets for drug repurposing, Nature. 583 (2020) 459–468. https://doi.org/10.1038/s41586–020-2286–9.
[43] C.M. Walker, G. Ko, Effect of Ultraviolet Germicidal Irradiation on Viral Aerosols, Environ. Sci. Technol. 41 (2007) 5460–5465, https://doi.org/10.1021/es070056u.
[44] M. Eickmann, U. Gravemann, W. Handke, F. Tolksdorf, S. Reichenberg, T. H. Müller, A. Seltsam, Inactivation of three emerging viruses – severe acute respiratory syndrome coronavirus, Crimean–Congo haemorrhagic fever virus and Nipah virus – in platelet concentrates by ultraviolet C light and in plasma by methylene blue plus visible light, Vox Sang. 115 (2020) 146–151, https://doi.org/10.1111/vox.12888.
[45] S.-M. Duan, X.-S. Zhao, R.-F. Wen, J.-J. Huang, G.-H. Pi, S.-X. Zhang, J. Han, S.-L. Bi, L. Ruan, X.-P. Dong, SARS Research Team, Stability of SARS coronavirus in human specimens and environment and its sensitivity to heating and UV irradiation, Biomed. Environ. Sci. 16 (2003) 246–255.
[46] H. Inagaki, A. Saito, H. Sugiyama, T. Okabayashi, S. Fujimoto, Rapid inactivation of SARS-CoV-2 with deep-UV LED irradiation, Emerg. Microbes Infect. 9 (2020) 1744–1747, https://doi.org/10.1080/22221751.2020.1796529.
[47] C.S. Heilingloh, U.W. Aufderhorst, L. Schipper, U. Dittmer, O. Witzke, D. Yang, X. Zheng, K. Sutter, M. Trilling, M. Alt, E. Steinmann, A. Krawczyk, Susceptibility of SARS-CoV-2 to UV irradiation, Am. J. Infect. Control 48 (2020) 1273–1275, https://doi.org/10.1016/j.ajic.2020.07.031.
[48] M. Raeiszadeh, B. Adeli, A Critical Review on Ultraviolet Disinfection Systems against COVID-19 Outbreak: Applicability, Validation, and Safety Considerations, ACS Photonics 7 (2020) 2941–2951, https://doi.org/10.1021/acsphotonics.0c01245.
[49] A.C. Walls, Y.-J. Park, M.A. Tortorici, A. Wall, A.T. McGuire, D. Veesler, Structure, Function, and Antigenicity of the SARS-CoV-2 Spike Glycoprotein, Cell. 181 (2020) 281–292.e6. https://doi.org/10.1016/j.cell.2020.02.058.

[50] D. Wrapp, N. Wang, K.S. Corbett, J.A. Goldsmith, C.-L. Hsieh, O. Abiona, B. S. Graham, J.S. McLellan, Cryo-EM structure of the 2019-nCoV spike in the prefusion conformation, Science 367 (2020) 1260–1263, https://doi.org/10.1126/science.abb2507.
[51] C.B. Jackson, M. Farzan, B. Chen, H. Choe, Mechanisms of SARS-CoV-2 entry into cells, Nat. Rev. Mol. Cell Biol. 23 (2022) 3–20, https://doi.org/10.1038/s41580-021-00418-x.
[52] A.M. Grishin, N.V. Dolgova, S. Landreth, O. Fisette, I.J. Pickering, G.N. George, D. Falzarano, M. Cygler, Disulfide Bonds Play a Critical Role in the Structure and Function of the Receptor-binding Domain of the SARS-CoV-2 Spike Antigen, J. Mol. Biol. 434 (2022), 167357, https://doi.org/10.1016/j.jmb.2021.167357.
[53] M.A.B. Larsen, A.B. Skov, C.M. Clausen, J. Ruddock, B. Stankus, P.M. Weber, T. I. Sølling, Cover Feature: Putting the Disulfide Bridge at Risk: How UV-C Radiation Leads to Ultrafast Rupture of the S-S Bond (ChemPhysChem 21/2018, 2805–2805, ChemPhysChem 19 (2018), https://doi.org/10.1002/cphc.201800908.
[54] A. Agarwal, J.K. Diedrich, R.R. Julian, Direct elucidation of disulfide bond partners using ultraviolet photodissociation mass spectrometry, Anal. Chem. 83 (2011) 6455–6458, https://doi.org/10.1021/ac201650v.
[55] C. Schöneich, Photo-degradation of therapeutic proteins: mechanistic aspects, Pharm. Res 37 (2020) 45, https://doi.org/10.1007/s11095-020-2763-8.
[56] Y. Shi, A. Zeida, C.E. Edwards, M.L. Mallory, S. Sastre, M.R. Machado, R.J. Pickles, L. Fu, K. Liu, J. Yang, R.S. Baric, R.C. Boucher, R. Radi, K.S. Carroll, Thiol-based chemical probes exhibit antiviral activity against SARS-CoV-2 via allosteric disulfide disruption in the spike glycoprotein, Proc. Natl. Acad. Sci. U.S.A. 119 (2022) e2120419119. https://doi.org/10.1073/pnas.2120419119.
[57] I.G. Madu, S. Belouzard, G.R. Whittaker, SARS-coronavirus spike S2 domain flanked by cysteine residues C822 and C833 is important for activation of membrane fusion, Virology 393 (2009) 265–271, https://doi.org/10.1016/j.virol.2009.07.038.
[58] D. Ray, L. Le, I. Andricioaei, Distant residues modulate conformational opening in SARS-CoV-2 spike protein, Proc. Natl. Acad. Sci. U. S. A 118 (2021), e2100943118, https://doi.org/10.1073/pnas.2100943118.
[59] Z.W. Tan, W.-V. Tee, F. Samsudin, E. Guarnera, P.J. Bond, I.N. Berezovsky, Allosteric perspective on the mutability and druggability of the SARS-CoV-2 Spike protein, Structure. 30 (2022) 590–607.e4. https://doi.org/10.1016/j.str.2021.12.011.
[60] G.M. Verkhivker, L.Di Paola, Dynamic Network Modeling of Allosteric Interactions and Communication Pathways in the SARS-CoV-2 Spike Trimer Mutants: Differential Modulation of Conformational Landscapes and Signal Transmission via Cascades of Regulatory Switches, J. Phys. Chem. B 125 (2021) 850–873, https://doi.org/10.1021/acs.jpcb.0c10637.
[61] S. Liu, G. Xiao, Y. Chen, Y. He, J. Niu, C.R. Escalante, H. Xiong, J. Farmar, A. K. Debnath, P. Tien, S. Jiang, Interaction between heptad repeat 1 and 2 regions in spike protein of SARS-associated coronavirus: implications for virus fusogenic mechanism and identification of fusion inhibitors, Lancet 363 (2004) 938–947, https://doi.org/10.1016/S0140-6736(04)15788-7.
[62] A. Sharir-Ivry, Y. Xia, Quantifying evolutionary importance of protein sites: A Tale of two measures, PLoS Genet 17 (2021), e1009476, https://doi.org/10.1371/journal.pgen.1009476.
[63] L. Orian, P. Mauri, A. Roveri, S. Toppo, L. Benazzi, V. Bosello-Travain, A. De Palma, M. Maiorino, G. Miotto, M. Zaccarin, A. Polimeno, L. Flohé, F. Ursini, Selenocysteine oxidation in glutathione peroxidase catalysis: an MS-supported quantum mechanics study, Free Radic. Biol. Med. 87 (2015) 1–14, https://doi.org/10.1016/j.freeradbiomed.2015.06.011.
[64] A. Sinz, Cross-Linking/Mass Spectrometry for Studying Protein Structures and Protein–Protein Interactions: Where Are We Now and Where Should We Go from Here? Angew. Chem. Int. Ed. 57 (2018) 6390–6396, https://doi.org/10.1002/anie.201709559.
[65] H.H. Wippel, J.D. Chavez, X. Tang, J.E. Bruce, Quantitative interactome analysis with chemical cross-linking and mass spectrometry, Curr. Opin. Chem. Biol. 66 (2022), 102076, https://doi.org/10.1016/j.cbpa.2021.06.011.
[66] P. Shah, G.A. Canziani, E.P. Carter, I. Chaiken, The Case for S2: The Potential Benefits of the S2 Subunit of the SARS-CoV-2 Spike Protein as an Immunogen in Fighting the COVID-19 Pandemic, Front. Immunol. 12 (2021), 637651, https://doi.org/10.3389/fimmu.2021.637651.
[67] J. Zhu, G. Xiao, Y. Xu, F. Yuan, C. Zheng, Y. Liu, H. Yan, D.K. Cole, J.I. Bell, Z. Rao, P. Tien, G.F. Gao, Following the rule: formation of the 6-helix bundle of the fusion core from severe acute respiratory syndrome coronavirus spike protein and identification of potent peptide inhibitors, Biochem. Biophys. Res. Commun. 319 (2004) 283–288, https://doi.org/10.1016/j.bbrc.2004.04.141.
[68] Y. Yu, Y.-Q. Deng, P. Zou, Q. Wang, Y. Dai, F. Yu, L. Du, N.-N. Zhang, M. Tian, J.-N. Hao, Y. Meng, Y. Li, X. Zhou, J. Fuk-Woo Chan, K.-Y. Yuen, C.-F. Qin, S. Jiang, L. Lu, A peptide-based viral inactivator inhibits Zika virus infection in pregnant mice and fetuses, Nat. Commun. 8 (2017) 15672, https://doi.org/10.1038/ncomms15672.